J Mater Sci: Mater Med (2009) 20:1677–1687
DOI 10.1007/s10856-009-3735-z

Formation of carbonated apatite particles from a supersaturated inorganic blood serum model

Karin Sandin · Lars Kloo · Pernilla Nevsten · Reine L. Wallenberg · Lars-Fride Olsson

Received: 21 August 2008 / Accepted: 16 March 2009 / Published online: 4 April 2009
© Springer Science+Business Media, LLC 2009

Abstract Pathological calcification is common among for instance dialysis patients, and this causes an increase in mortality risk. An elevated serum phosphate concentration among those patients strongly correlates to this increase. In this work investigations of the conditions, composition, crystallinity and morphology of in vitro calcification are performed and related to results from in vivo studies. The study was performed under conditions mimicking physiological ones, i.e. a pH around 7.40, a temperature of 37°C, an ionic strength of 150 mM and ion concentrations close to those in human serum including the effects of elevated phosphate concentrations. The course of precipitation involves an initial precipitate that subsequently re-dissolves to give another precipitate, in accordance with the well-known Ostwald ripening theory. The final bulk precipitate consists of a macroscopically amorphous carbonated apatite. The amorphous apatite is formed from assemblies of spherical particles in the μm range, in turn composed of nano-crystalline needles of about 10×100 nm. Even the initially formed precipitate, as well as a small amount of precipitate that occurs on the liquid surface, consist of a carbonated calcium phosphate. The in vitro observed carbonated apatite bears strong resemblance to in vivo cardiovascular calcification known from literature.

K. Sandin · L.-F. Olsson
Gambro Corporate Research, Lund, Sweden

K. Sandin · L. Kloo (✉)
Department of Chemistry, Royal Institute of Technology, Stockholm, Sweden
e-mail: Larsa@kth.se

P. Nevsten · R. L. Wallenberg
nCHREM (National Center of High Resolution Electron Microscopy), Lund University, Lund, Sweden

1 Introduction

Human vascular deposition of solid calcium phosphates, so called pathological calcification, is a severe and common problem among elderly and is also related to pathological conditions, such as kidney diseases and thus dialysis patients [1]. The calcification is connected to an increased mortality risk in cardiovascular diseases [2]. Classical risk factors for vascular calcification include age, male gender, smoking, inflammation, hypertension, dyslipidemia, and diabetes. Dialysis patients are subjected to additional risk factors, such as inflammation [3] and imbalance in the concentrations of calcium and phosphate in the blood. An elevated serum phosphate concentration among dialysis patients is strongly correlated to an increase in mortality risk [4].

Several in vitro studies have been performed in order to investigate calcium phosphate precipitation under conditions imitating physiological conditions. However, the conditions used have usually deviated from physiological ones regarding for instance pH, temperature, ionic strength and electrolytes. Some examples are given in Refs. [5–8]. In this work, we report precipitation experiments carried out under conditions more close to physiological conditions, i.e. a pH around 7.40, a temperature of 37°C, and an ionic strength of 150 mM with sodium chloride and bicarbonate as ionic medium and calcium and phosphate concentrations close to those in human serum. The purpose has been to investigate which calcium phosphate phase(s) that will form under such conditions. Also, long-term experiments have

been carried out with calcium and phosphate concentrations even closer to human ones [9, 10].

2 Experimental procedure

2.1 Preparation of solutions

Stock solutions with an ionic strength of about 150 mM were prepared from distilled water and salts purchased from Merck. All salts were of pro analysi grade, except NaCl that was of suprapur grade. The model system was kept as simple as possible in order to avoid unanticipated interactions from other serum components. The salts included were sodium chloride (NaCl), sodium bicarbonate ($NaHCO_3$), calcium chloride ($CaCl_2 \cdot 4H_2O$) and sodium phosphate (20 mol% $NaH_2PO_4 \cdot H_2O$ and 80 mol% $Na_2HPO_4 \cdot 2H_2O$, pH 7.4). The ion concentration of the calcium chloride stock solution was determined to 49.7 mM by titration of the chloride ions using a calibrated silver nitrate solution, and the concentration of the phosphate stock solution was determined to 52.1 mM by acid-base titration.

2.2 Precipitation

Stock solutions of sodium chloride, bicarbonate, and phosphate were mixed in a glass container, pH was adjusted to 7.40 (see below), and the temperature was kept at 37 ± 1°C by a thermostat. An appropriate volume of the calcium stock solution was added, which defined the starting point ($t = 0$) of the experiment. The total volume in the container was 150 ml and the solution was stirred with a magnetic stirring bar at the rate of 500 rpm. The concentrations of the ions used are shown in Table 1, as are the concentrations of the inorganic components in serum of normal subjects [11] and dialysis patients [12]. The ionic strength and pH in the solutions were almost the same as in serum (about 150 mM and 7.40). The phosphate concentration used is comparable to concentrations in serum of dialysis patients, i.e. somewhat higher than in normal subjects. The concentration of calcium was 2.6 mM, and thereby the free calcium ion concentration about 1.8–1.9 mM when complex formation is taken into consideration [$CaHCO_3^+$ and $CaHPO_4$(aq), see the Appendix]. Measurements using the calcium ion-selective electrode showed a higher value; around 2.3–2.5 mM). The calculated value of 1.8 mM represents an elevated value of about 50% compared to the free calcium concentration of serum. The bicarbonate concentration used was in the lower region of serum concentrations, 21.5 mM, in order to ensure that formation of $CaCO_3$(s) was avoided (calculations using suitable equilibrium constants indicate that formation of $CaCO_3$(s) is not expected, see the Appendix). pH was kept constant by means of the buffer carbonic acid/bicarbonate. Since there is an equilibrium between the acid-base components, and a small leakage of CO_2 is inevitable in the equipment set-up used, the carbonic acid concentration tend to decrease and thus pH to increase. In order to suppress this effect, the system was connected to a gas flask, providing constant addition of 5% CO_2 (g) in N_2(g) via a glass capillary ending above the solution surface. This resulted in a pH of about 7.40 ± 0.02 at the beginning and end of the experiments. The cover was also sealed with rubber plugs in order to minimize gas leakage.

Table 1 Free ion concentration (conc) in human serum in healthy individuals [11] and patients on dialysis [12] and the concentrations used in this study

	Human free ion conc		Conc in this study	
	Healthy individuals	Dialysis patients	Total ion	Free ion
Ca^{2+}	1.2–1.3	1.1–1.4	2.6	1.8–1.9
Mg^{2+}	0.4–0.5		0	0
HPO_4^{2-} and $H_2PO_4^-$	0.7–1.4	1.0–3.0	1.9–3.5	1.7–3.2
HCO_3^-	21–30		22	21
Na^+	135–145		138–140	138–140
K^+	3.5–4.7		0	0
Cl^-	98–108		116–120	116–120
pH	7.37–7.45	7.33–7.51	7.38– 7.42	

All concentrations are in mM. Phosphate mainly exists in the forms HPO_4^{2-} (about 80%) and $H_2PO_4^-$ (about 20%). The human pH was measured arterially and the pH in this study is initial/final. The free ion concentrations in this study is estimated from known equilibrium constants [33] (see Appendix)

2.3 Instrumentation

pH was monitored by a standard glass electrode, which was calibrated before each experiment. The free calcium ion concentration was recorded with an ion selective electrode, Orion 97–20 ionplus®. The total calcium and phosphate ion concentrations in the solutions were determined intermittently by reflectance spectrophotometry using a KODAK Ektachem DTII (Eastman Kodak Company, Rochester, New York, US) equipment, calcium in the form of its Arsenazo III dye complex at 680 nm and phosphate through its molybdenum complex at 660 nm. Since the intended use of the equipment is for measurements on plasma, the values were slightly corrected using calibration curves.

The formation of particles was monitored by means of a particle sensor (see Fig. 1) that continuously recorded the course of precipitation. The sensor technique is based on

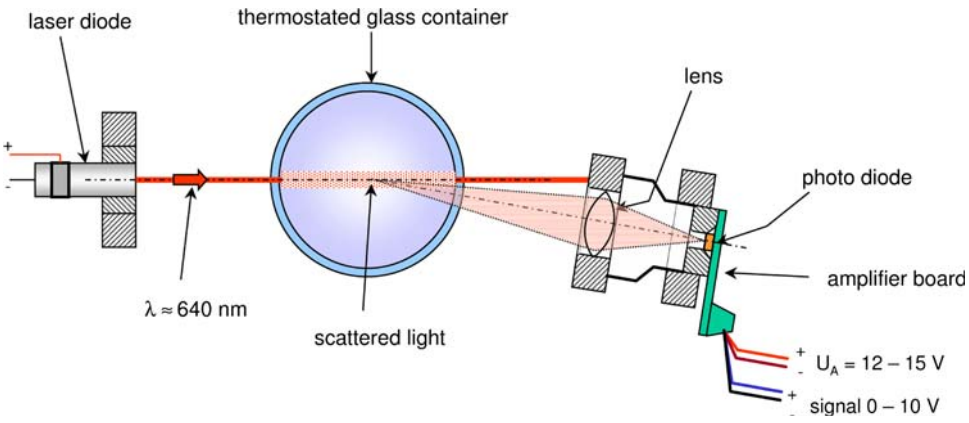

Fig. 1 A picture of the particle sensor, used to follow the course of precipitation

elastic light scattering by particles, and an increase in signal level implies a greater amount of particles or particles of larger size. Intermittently, the particle sensor was supplemented by a particle counter, which allowed the amount of particles of different size fractions to be determined. Aliquots of 5 ml were excerpted, diluted with distilled, microfiltered (0.2 μm) water to an appropriate particle concentration (dilution 4–20 times), and then immediately analysed on a HIAC Particle Counter System Model 9703 providing the particle size distribution. Light microscopy images of the precipitate in solution were recorded on a ZEISS Axioskope 2 microscope with an AxioCam MRc5 camera immediately after excerption. The precipitate was collected by filtration onto 0.45 μm nitro cellulose filters (Schleicher & Schuell), washed with small portions of distilled water at 4°C and then allowed to dry at room temperature.

After dissolution of the precipitate in concentrated nitric acid and appropriate dilution in distilled water, the total calcium concentration was determined by atomic absorption spectrometry (AAS), using a Varian SpectrAA 220FS spectrometer with a hollow cathode lamp operating at 422.7 nm, and the total phosphate concentration spectrophotometrically in the form of its molybdenum complex at 882 nm using a Perkin-Elmer Lambda 20 spectrophotometer. Particles were scraped off the filter paper onto lacey carbon film copper grids (Oken Shoji) or, when the presence of carbon was determined, onto copper grids with Silicon Monoxide Type-A film with removed Formvar support film (Ted Pellas). The morphology of the particles and their diffraction pattern were examined with transmission electron microscopy (TEM) on a JEOL 3000F microscope. Evaluation of the patterns was performed by calculating the radial intensity distribution (script for digital micrograph downloaded from ftp.gatan.com). The background was manually subtracted. X-ray energy dispersive spectrometry (XEDS) was performed with a INCA Oxford instrument spectrometer, in order to determine the elemental composition. Powder X-ray diffraction was performed on a PANalytical X'Pert Pro diffractometer using Cu Kα radiation. FT-IR (Fourier transformation infrared) transmission spectra were recorded on a Perkin-Elmer spectrum BX FTIR instrument with an effective spectral range from 450 to 4400 cm^{-1}, using KBr as matrix (0.1–5 mg sample/200–400 mg KBr). Raman-spectroscopic measurements were performed on a Renishaw System 1000, equipped with a He/Ne (633 nm) laser, DMLM Leica microscope, and a CCD detector. Total carbon content analysis was performed by MikroKemi AB in Uppsala, Sweden, where the sample was heated to 1800°C, the combustion gases were separated by gas chromatography, and the released CO_2 was subsequently determined with a thermal conductivity detector. Thermogravimetric analysis (TGA) up to 900°C was performed on a Perkin-Elmer Thermogravimetric Analyzer, TGA 7.

One additional control experiment was performed with a cell culture medium (RPMI 1640, Invitrogen) containing amino acids, vitamins, glucose, and inorganic ions. Besides the ions used in the experiments described earlier, magnesium, potassium, nitrate, and sulphate were included as well. The total calcium and phosphate ion concentrations were 2.9 mM and 5.1 mM, respectively.

3 Results

3.1 The course of precipitation

The induction time, which is the time that has elapsed from mixing of the electrolytes until the precipitate forms, is highly dependent on the degree of supersaturation. In Fig. 2 the stepwise shape of the curve recorded using the particle sensor is shown. The time T1 is defined as the time where the first peak starts in the particle sensor curve and the time T2 as the time where the second peak starts; the latter being more distinct than the former. Higher supersaturation results in a faster precipitation reaction, e.g. the higher the phosphate concentration the shorter the

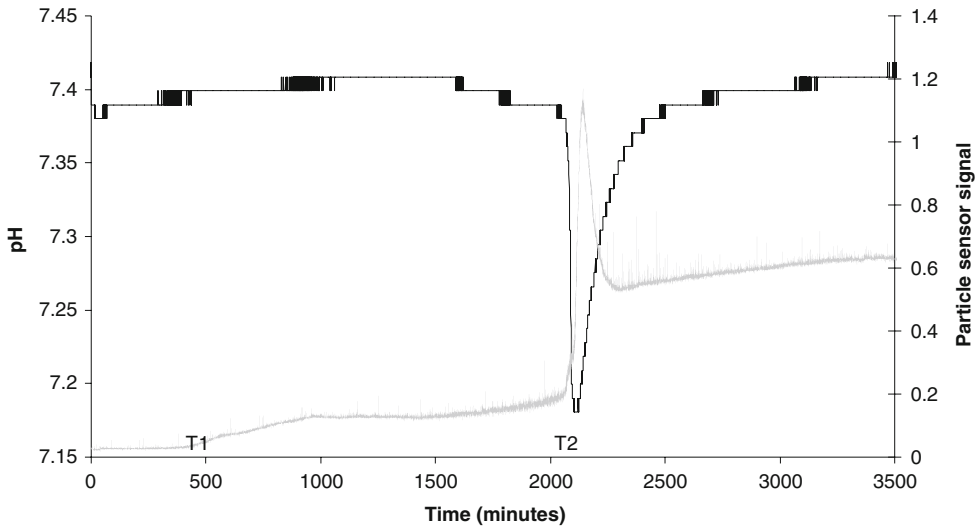

Fig. 2 Typical time variation of the particle sensor curve (*grey curve*). Time 0 was set to the time when the calcium solution was added to the solution, time T1 set to the time where the curve starts to increase for the first time and time T2 to the time where the curve starts to increase for the second time (more distinctly than T1). pH remains at approximately 7.40, except around T2, where it drops to 7.1 (*black curve*). The total phosphate concentration used was 2.1 mM

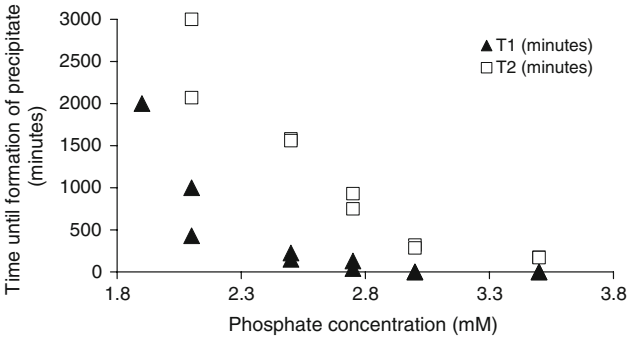

Fig. 3 Variation of T1 and T2 with phosphate concentration. For definitions of T1 and T2, see text and Fig. 2

induction time, as shown in Fig. 3. The difference between T1 and T2 decreases with increasing phosphate concentration. Figure 4a shows an example of the variation in pH, free and total calcium ion concentration, and total phosphate concentration together with the light scattering signal from the particle sensor. The elapsed time until particle formation (T1) is recorded by the particle sensor varies from zero minutes up to several hours (0 min in Fig. 4a) depending on the phosphate concentration used. No marked calcium and phosphate concentration changes are observed before T2 as the precipitation proceeds, except in the case of the highest phosphate concentration. In most cases, the particle sensor signal slowly reaches a local maximum and then tends to decrease (at around 200 min in Fig. 4a). The existence of a first maximum was also confirmed with measurements using the particle counter (see Fig. 4b). After around 240 min, pH and the free calcium ion concentration start to decrease slowly (see Fig. 4a), and at around 290 min there is a sharper drop in the calcium concentration. At around 320 min time T2 is reached, marked by a strong increase in the particle sensor signal, and approximately at the same time the pH reaches a

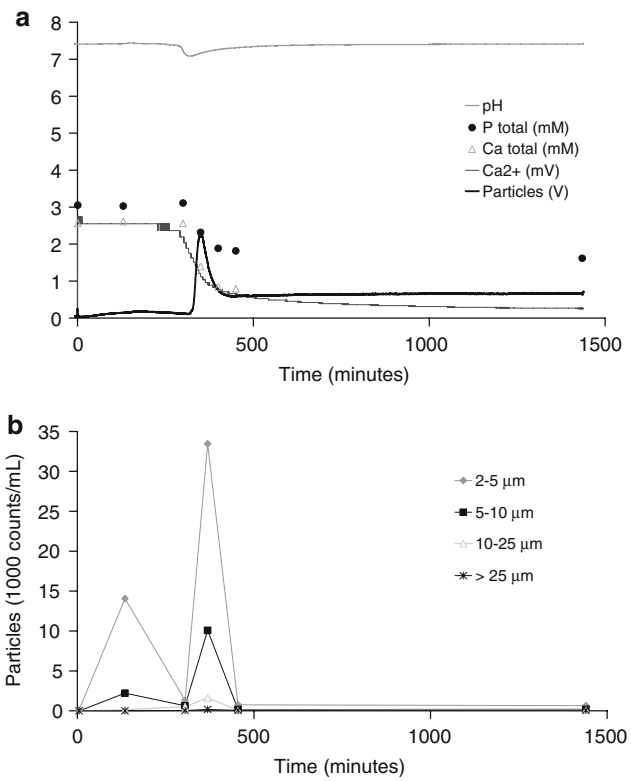

Fig. 4 **a** The variation of pH, total phosphate concentration, total and free calcium ion concentration, and particle sensor signal with time. **b** Results from the particle analysis showing the amounts of different size fractions of the precipitated particles. The total phosphate concentration used was 3.0 mM

temporary minimum and then slowly returns to its original value [note that pH is buffered by $CO_2(g)$]. pH drops to 7.11 ± 0.08 for all phosphate concentrations studied, and there is no trend to higher or lower value with increasing phosphate concentration. The delay from the start in the decrease in calcium concentration, i.e. consumption of

calcium ions, until a signal from the particle sensor is detected is probably due to the particles first formed are too small to be detected ($\leq \sim 0.3$ μm). The later (after T2) slow decrease in the particle sensor signal is probably caused by particles sticking to the electrodes and the walls of the container, which both decrease the number of particles in solution and blocks the laser light. In all cases, the smallest particle fraction possible to characterise with the particle counter, 2–5 μm, dominates (see Fig. 4b). This shows that the increase in light scattering signal is caused by an increase in number but not necessarily by an increase in size of existing particles.

The course of precipitation seems not to be markedly affected by a lowered stirring rate or by usage of another buffering gas mixture [5% CO_2 (g), 76% N_2 (g) and 19% O_2 (g)]. A slightly lowered initial pH tends to slow the process down somewhat, but without affecting the appearance of the particle sensor curve. Accordingly, a slightly increased pH speeds up the process. When the experiments were performed at a constant phosphate concentration (instead of a constant calcium concentration), the higher the calcium concentration was, the faster the precipitation occurred; i.e. these results are analogous to the results obtained when the phosphate concentration was varied.

3.2 Precipitate composition

AAS (Ca) and spectroscopic analyses (P) of the bulk precipitate obtained after T2 show a composition of 35.2 wt% Ca and 16.5 wt% P, corresponding to a Ca/P molar ratio of 1.65. Within experimental errors, XEDS measurements confirm this ratio, giving a Ca/P molar ratio of about 1.6. However, the Ca/P molar ratio of the initial precipitate retrieved before T2 is 1.8, as determined by XEDS measurements. In all experiments performed, a precipitate consisting of thin flakes on the liquid surface also appeared. This precipitate also shows a Ca/P molar ratio of about 1.8, according to XEDS measurements.

The Ca/P molar ratio of the consumed calcium and phosphate, i.e. $([Ca^{2+}]_{start} - [Ca^{2+}]_t)/([P]_{start} - [P]_t)$, where $[Ca^{2+}]$ is the calcium ion concentration and [P] is the phosphate concentration at the start of the experiment and at time t, was calculated in two different ways. Depending on the technique of calcium ion determination, Ca/P molar ratios of about 1.6 ± 0.3 (reflectance spectrophotometry) or 1.8 ± 0.2 [ion-selective electrode corrected for additional ions existing as complexes (see Appendix)], are obtained. No trend towards higher or lower Ca/P molar ratio with increasing phosphate concentration is inferred. Before T2, the changes in measured calcium and phosphate concentrations were too small to allow any reliable estimation of the molar ratio of consumed Ca/P.

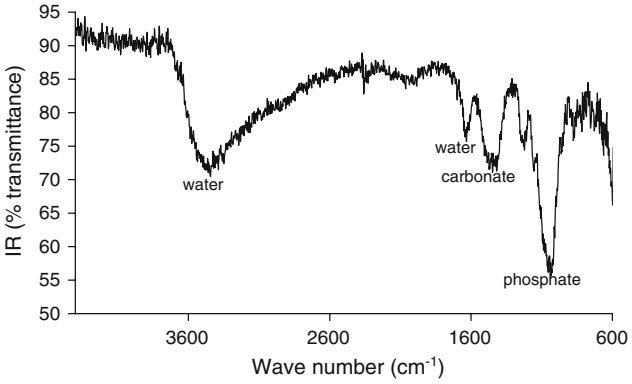

Fig. 5 A typical IR spectrum of the bulk precipitate showing bands originating from phosphate, carbonate and water components. Precipitates prepared from different phosphate concentration all show a similar appearance

The typical IR spectra of bulk precipitate obtained after T2 (see Fig. 5) exhibit rather featureless peaks and are dominated by bands that can be assigned to vibrations from phosphate, carbonate and water components. Bands originating from the phosphate ion, PO_4^{3-} are observed at 962, 1032, 1054, 1088 cm^{-1}, as in hydroxyapatite [13] and carbonated apatite [14]. Bands at 754, 876, 1418, 1446 and 1466 cm^{-1} can be attributed to CO stretching modes of carbonate in carbonated apatite [14]. The band around 3400 cm^{-1} probably originates from OH stretching modes of water molecules. In spectra of octacalcium phosphate [$Ca_8H_2(PO_4)_6 \cdot 5H_2O$], a weak band around 1632 cm^{-1} is attributed to H_2O bending modes [15]. Since the strong bands of HPO_4^{2-} stretching vibrations at 1109 and 1118 cm^{-1} [15] were not observed in this study, our precipitate can not be composed of octacalcium phosphate. However, the band at 1632 cm^{-1} probably originates from water, and the fact that the signal is rather strong indicates a rather large incorporation of water in the precipitate, which is also confirmed by the results from TGA measurements (see below). Additional weak bands and a stronger band at 1220 cm^{-1} are observed but can not be unambiguously assigned. The IR spectrum of the surface precipitate has the same appearance as the bulk precipitate obtained after T2, although bands around 1220 and 1152 cm^{-1} are on a relative scale stronger in the surface precipitate.

The totally symmetric stretching of PO_4^{3-}, v_1, at about 962 cm^{-1} dominates the Raman spectra of carbonated apatite [16]. This band was observed for all the examined precipitates, although it was most prominent for the bulk precipitate obtained after T2, a bit less for the initially formed precipitate obtained before T2, and even less for the precipitate obtained on the liquid surface in the container. The spectra show signs of decomposition caused by laser radiation, probably due to evaporation of water molecules.

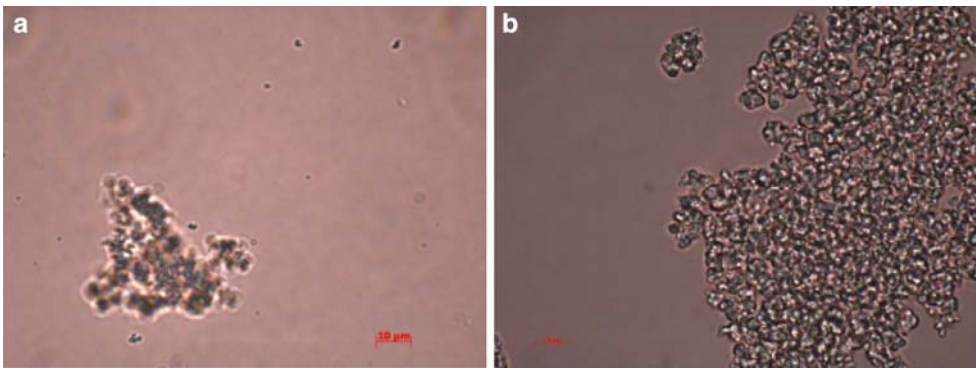

Fig. 6 Light microscopy images before **a** and after **b** T2. In both cases, the precipitates consist of μm-sized rather spherical particles assembled together. The amount of particles was on the whole larger after T2 and the assemblies consist of larger amounts of particles

The analysis of total carbon content showed the presence of 1.2 wt% carbon in the bulk precipitate. XEDS measurements also confirmed the presence of carbon and oxygen, although it is not possible to make any reliable quantification.

A loss of about 15 wt% water from the bulk precipitate is observed using TGA. The steady loss of mass without distinct steps at specific temperatures indicates a structurally non-ordered incorporation of water. It cannot be excluded that a small part of the weight loss originates from release of CO_2 from carbonate, at least at the higher temperatures used.

3.3 Structure of precipitate

The appearance of the precipitate in the solution where it was formed, before and after T2, was examined using light microscopy (see Fig. 6). In both cases, the precipitates consist of assembled μm-sized rather spherical particles. However, after T2 the assemblies consist of larger amounts of particles. The amount of particles on the whole was larger after T2, which was confirmed by particle count determinations (see Fig. 4b). The fact that the μm-sized particles are spherical makes the particle count determinations reliable, at least in the 2–5 μm fraction, since this technique of determination is partly dependent on particle shape.

Powder X-ray diffractograms show broad peaks emerging from the precipitates (Fig. 7). This indicates the presence of very small crystallites. The diffraction peaks observed might at least partly be caused by exposure to X-ray radiation, since induced slow evaporation (of water) may initiate a crystallisation process. In terms of crystallite dimensions, some indications can be deduced from the peak width. Essentially only the peak at about 27 degrees is sharp and can be assigned to the [002]-reflection of hydroxyapatite [17]. Although this is a single clear assignment, it is an indication that the crystallite is extended further along the c-axis is longer than the other two dimension and consistent with the TEM data obtained (vide infra).

TEM analysis of the bulk precipitate obtained after T2 shows that needles typically 10 nm wide and 100 nm long form the spherical particles in the μm range (see Fig. 8a, b). The diffraction pattern (see Fig. 8c) indicates a nano-crystalline material. Concerning the initial precipitate

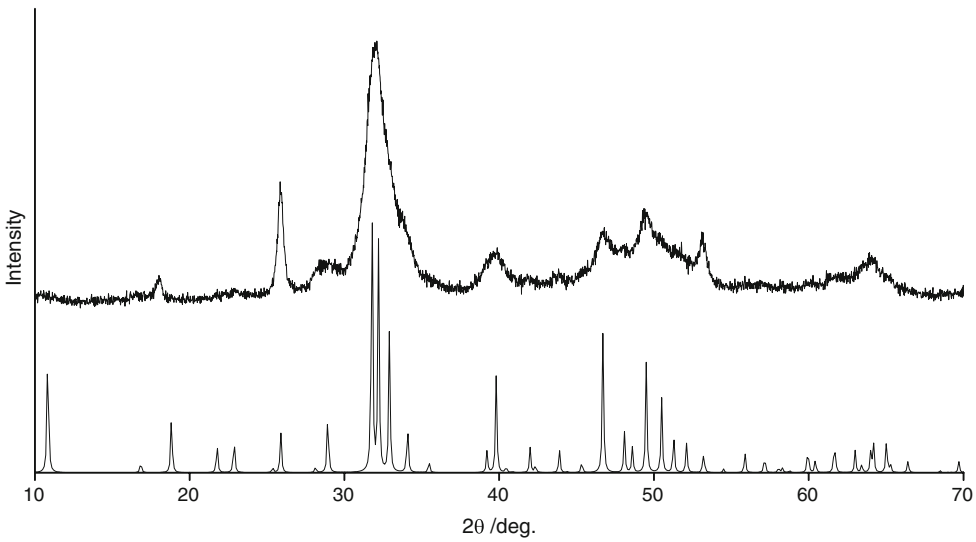

Fig. 7 Powder X-ray diffractogram of the bulk precipitate (*top*) showing signs of sub-micrometer crystalline particles. For comparison, also the diffraction pattern generated from structure data of a synthetic hydroxyapatite is included (*bottom*) [17]

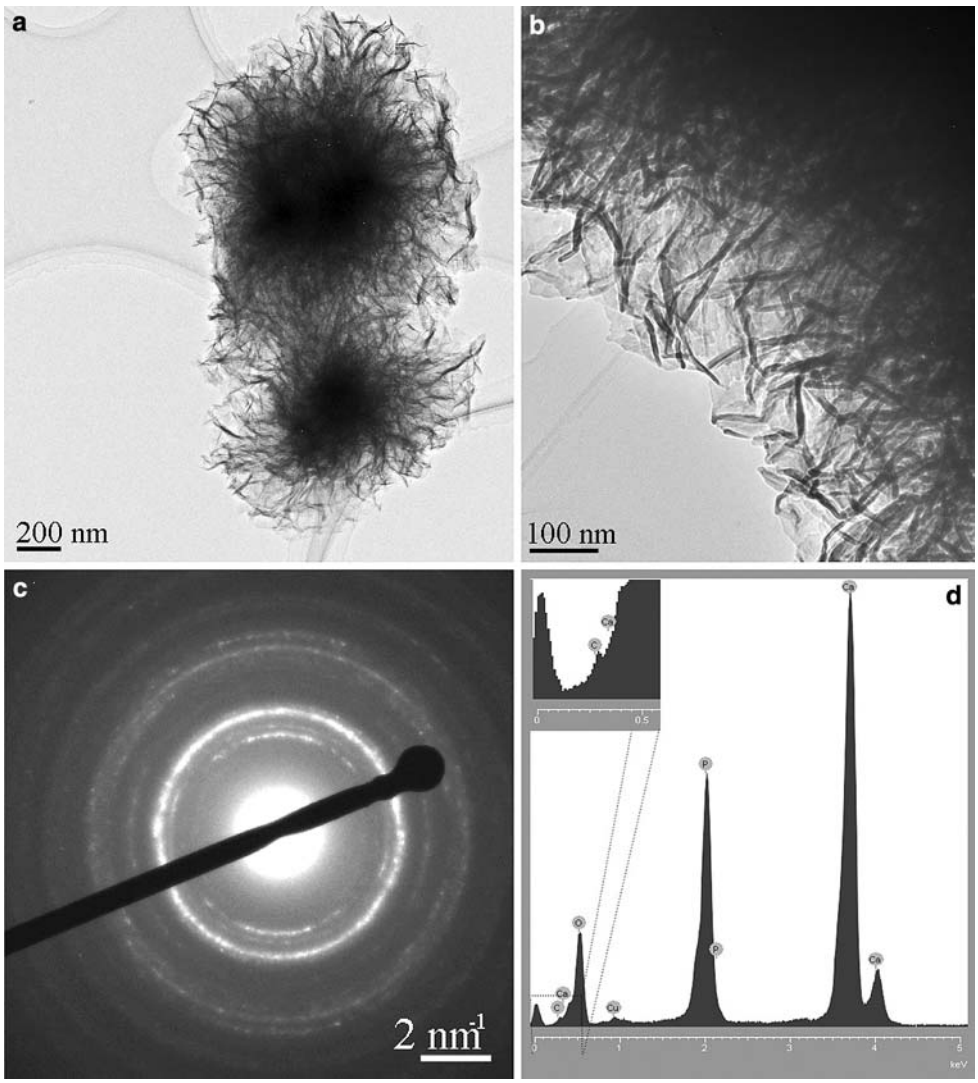

Fig. 8 **a** TEM image of the bulk precipitate obtained after T2 showing needle-like particles, typically 10 nm wide and 100 nm long, merge to form spherical particles in the μm range; **b** higher magnification of a; **c** the diffraction pattern from an edge of a particle, indicating a nano-crystalline material with a slight orientational (radial) order shown by the incomplete circles; **d** typical XEDS spectrum showing the elements present; P, Ca and O, and some C (the Cu signal is from the sample grid holder)

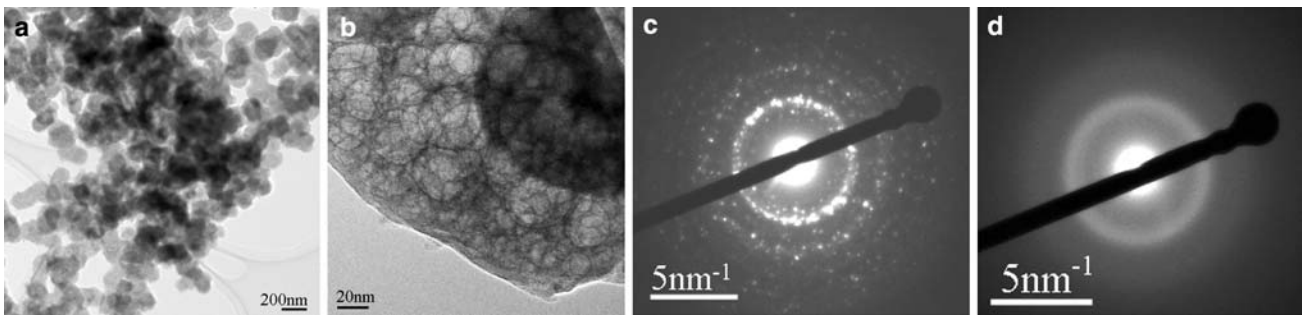

Fig. 9 **a** TEM image of the initial precipitate obtained before T2; **b** higher magnification of a; the thin circles in the image are probably spherical voids formed due to evaporation of the sample caused by electron beam damage; **c** diffraction pattern from an edge of a particle contains many close reflections, probably caused by the presence of several crystalline phases or sample decomposition; **d** diffraction pattern from the centre of the sample giving the impression of a rather amorphous material

obtained before T2, if the measurements are performed on the middle of a particle assembly, the diffraction pattern gives the impression of the material being amorphous. However, measurements on the thin edges indicate the presence of crystalline material, although consisting of crystallites smaller than those in the bulk precipitate obtained after T2. The appearance is different from the bulk precipitate (see Fig. 9a, b) and the lattice spacing

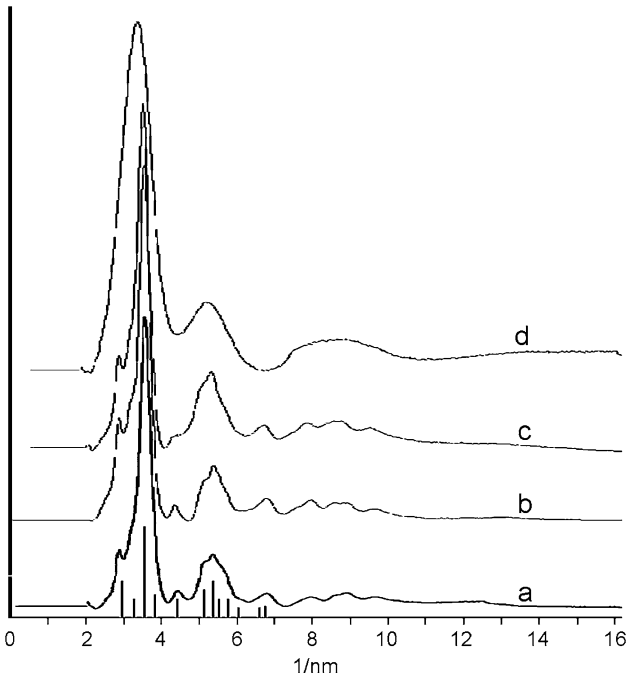

Fig. 10 Radial intensity distributions calculated from the diffraction patterns, showing the lattice spacings of the crystals; (a) surface precipitate; (b) bulk precipitate; (c) the edge of an initial precipitate; and (d) the centre of an initial precipitate, as compared to intensity peaks of reference values of hydroxyapatite [19]

shows additional diffraction spots (see Fig. 9c). The many close reflections are probably caused by the presence of several crystalline phases or sample decomposition because of electron beam damage. This precipitate is also more sensitive to radiation and spherical voids are formed when the sample is exposed to the electron beam (see Fig. 9b), probably due to local heating leading to evaporation of H_2O and/or CO_2 from the solid sample. The TEM image corresponds well to the appearance of a TEM image of amorphous calcium phosphate [18]. TEM on the thin surface precipitate seems to indicate a mixture of the appearance and properties of the precipitates obtained before and after T2. The distances between the crystal faces, d, observed in the diffraction pattern from the crystals of the three types of precipitate correspond rather well to those of hydroxyapatite [19], as seen in Fig. 10.

Despite the addition of the components in the cell culture medium, i.e. additional inorganic ions, amino acids, vitamins, and glucose, the same appearances of the particle sensor curve and pH changes as for the original experiment were observed (see Fig. 11).

4 Discussion

The course of precipitation monitored by the particle sensor indicates that a first phase forms, dissolves, at least partly, and then a subsequent formation of a second phase takes place (see Fig. 4). According to Nancollas [20], it is generally accepted that biological precipitation involves deposition of lattice ions but also concomitant dissolution of precursor phases. This is also in accordance with the Ostwald ripening theory [21], which implies that when a system crystallizes, it often forms metastable phases first and then transforms in successive stages, in which the free energy is lowered. However, the phases in this study are not obviously crystalline. Just as in the present study, Boulet et al. [7] found the precipitation to take place in two steps, with a first gelatinous and a second granular precipitate. However, in the present study, the gelatinous/granular appearance was not observed.

In the literature, detected changes in pH are often associated with precipitation in a non-buffered system [7], e.g. with potentiostatic methods, in which the time of precipitation is related to hydroxide consumption in order to keep the pH constant [8, 22]. As shown in Fig. 4,

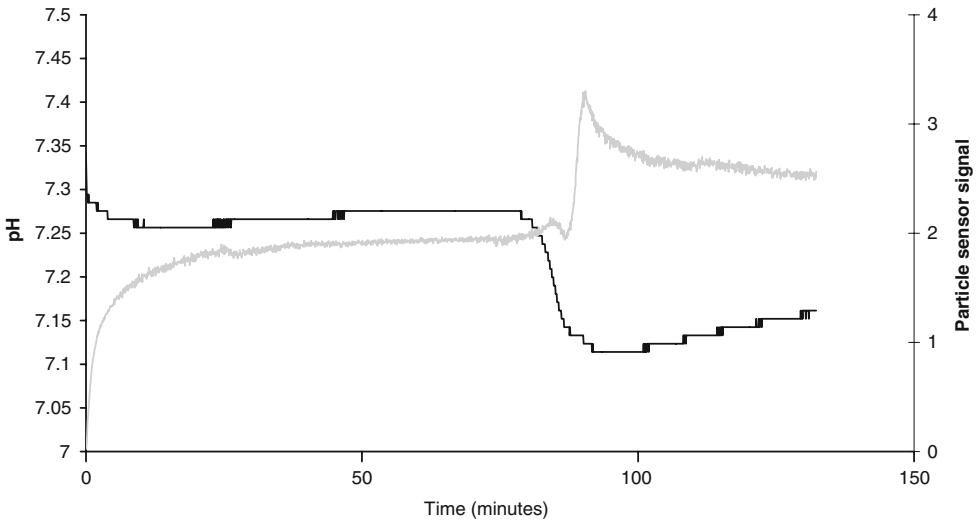

Fig. 11 The variation of pH (*black curve*) and particle sensor signal (*grey curve*) with time in a culture medium. The course of precipitation seems to be analogous to that observed for the other experiments performed on a fully inorganic serum model

a precipitate has already formed when the drop in pH is recorded, and accordingly, when using a potentiostatic method, whatever happens before the drop in pH will be missed.

As concluded from AAS, spectroscopic measurements, IR and Raman analyses, and analysis of total carbon content, the bulk precipitate formed in this study consists of a carbonated apatite and light microscopy investigations show it to consist of assemblies of spherical particles in the μm range. The broad peaks in X-ray diffractograms suggests a structure based on quite small crystallites, and TEM analyses show that the spherical μm-assemblies are composed of nano-crystalline needles in the 10×100 nm range. The poor macroscopical crystallinity of the precipitate might be due to the high, almost physiological, level of hydrogen carbonate present in the solution. Dorozhkin et al. obtained poorly crystalline carbonated hydroxyapatite in a precipitation study and found that a higher concentration of hydrogen carbonate results in a less crystalline apatite [5]. It is known that substituted apatites show an increasing degree of disorder and incommensurate behavior [23].

Earlier precipitation studies of calcium phosphates performed in a medium, not containing the physiological bicarbonate buffer, have shown the precipitate to consist of hydroxyapatite [6–8]. Although the precipitation method used in this study is rather physiological, the solutions utilized are simplified as compared to the inorganic part of the serum regarding the ions present. However, the result from the experiment performed in culture medium indicates that the presence of additional physiological ions and other compounds does not markedly affect the precipitation process. Experiments with four times higher concentration of revised simulated body fluids performed by Dorozhkin et al. [5] showed that with additional ions present, and with markedly increased ion concentration, the resulting precipitate is still a carbonated apatite. The formation of a carbonated apatite in vitro is of special interest, since this is the substance generally reported as pathological cardiovascular calcifications in vivo [24–27]. Becker et al. [24] claimed that biological carbonated apatite in atherosclerotic plaques is in a nano-crystalline form with particles of about 20 nm in size, i.e. in about the same dimensions as in this work. Kim et al. showed that the surfaces of sintered hydroxyapatites soaked in simulated body fluid undergo structural changes and crystallize into bone-like apatite [28] with a TEM appearance similar to the appearance of the bulk precipitate in this study.

In a similar study, in which solutions were stored and maintained for several months without stirring, we also found that the precipitate formed was a carbonated apatite with a suggested composition $Ca_5(PO_4)_3(HCO_3) \cdot 4H_2O$ [10]. In contrast to this study, precipitate formation involving several steps was not obvious. The concentrations of calcium and phosphate in the precipitates were slightly lower (32.9 wt% calcium and 15.4 wt% phosphate), although the Ca/P molar ratio was still 1.65. The carbon content was a bit higher (2 wt% as compared to 1.2 wt%). The IR bands were slightly different and shifted. Possibly, no well-defined carbonated apatite with a specific composition forms in aqueous solution containing calcium, phosphate, carbonate, sodium and chloride ions. Instead, the composition may be dependent on the individual concentrations of the ions and local variations. Thus, external conditions and variations in stirring may slightly influence the composition of the product formed.

Besides the bulk precipitate obtained after T2, two other types of precipitates are formed; the one initially formed and the one appearing on the liquid surface. Both phases have a slightly higher Ca/P molar ratio (1.8) as compared to the bulk precipitate (Ca/P molar ratio about 1.65). The Ca/P molar ratio of 1.8 does not correspond to any known specific crystalline calcium phosphate, but it is probably composed of a carbonated apatite with a higher carbonate content as compared to the bulk precipitate. Although the surface precipitate and the initial precipitate have about the same Ca/P molar ratio, we have not been able to conclude whether they have exactly the same composition. The surface precipitate forms flakes that float on the surface. This is a trivial but rather interesting observation. Robinson, in his early electron microscopy work on apatites and bone minerals, pointed out that carbonated apatites tend to form plate-like crystals, rather than needles as hydroxyapatite. Possibly, the flakes or plate-like appearance of the surface precipitate is a consequence of a higher carbonate content [29].

Our study clearly shows that a precipitate is initially formed and then re-dissolves to give another precipitate. The drop in pH occurring during the dissolution stage indicates that H^+ is released from an ion incorporated in the initial precipitate, most likely HPO_4^{2-} and/or HCO_3^-. The TEM measurements indicate that the initial precipitate obtained before T2 is less crystalline.

Regarding the surface precipitate, an observation of a band from about 1150 cm^{-1} to about 1250 cm^{-1} in IR spectra can been attributed to the bending mode of HPO_4^{2-} [30]. This might indicate that some of the PO_4^{3-} is present as HPO_4^{2-}, in contrast to the bulk precipitate obtained after T2. However, the Ca/P molar ratio calculated from the XEDS measurements imply a lower amount of phosphate per calcium, and not a higher, which would be the expected observation in the case of incorporation of an ion with lower negative charge. The higher Ca/P molar ratio for the surface precipitate could instead indicate an exchange of some of the PO_4^{3-} ions for other ions, probably CO_3^{2-} or HCO_3^-. Since the precipitate is in direct contact with the

gas above the liquid surface, containing CO_2(g), incorporation of more carbonate and especially HCO_3^- is highly plausible.

5 Conclusions

Although many researchers claim that calcification is a regulated process similar to the bone formation process, involving matrix proteins [31, 32], this is not necessarily a complete explanation. It is clear that the same type of calcium phosphates are formed, i.e. an nano-crystalline carbonated apatite, under physiological in vitro conditions.

Acknowledgements Hans Hallstadius, former employee at Gambro's Development Department, is acknowledged for constructing the particle sensor and Andreas Fischer at the Department of Chemistry, Royal Institute of Technology, Stockholm, Sweden, for performing the TGA and X-ray diffraction investigations. This project was supported by a grant from the Swedish Research Council (VR 621-2001-3653).

Appendix

Concentrations were calculated by an in-house program system utilizing known equilibrium constants [33] for the conditions used. These data include complex formation, acid-base equilibrium, and solubility. When necessary, the values were corrected to apply to an ionic strength of 150 mM. The formation of complexes between calcium, phosphate and bicarbonate ions were taken into consideration. $H_2PO_4^-$ (20%) and HPO_4^{2-} (80%) are the dominating forms of orthophosphoric acid at pH 7.4. The other components, H_3PO_4 and PO_4^{3-} were neglected. In the carbonate system, HCO_3^- dominates ($\sim$95%); the other components are dissolved carbon dioxide ("carbonic acid") CO_2(aq) and the carbonate ion, CO_3^{2-}. Since the concentration of the latter is <0.2 mM, the formation of the complex $CaCO_3$(aq) was neglected. The acid constant $pK_{a2} = 6.7$ for the acid-base pair $H_2PO_4^-/HPO_4^{2-}$. For the hydrogen carbonate system, the values have been obtained by interpolating between ionic strength 0.1 and 0.2 mM resulting in $pK_{a1} = 6.07$ for CO_2(aq)/HCO_3^- and $pK_{a2} = 9.75$ for HCO_3^-/CO_3^{2-}. The dissociation constant of water employed was $pK_w = 13.4$. Only the complexes $CaHPO_4$(aq) and $CaHCO_3^+$ with complex formation constants, logK, 1.9 and 1.1, respectively, were included.

References

1. Hujairi NMA, Afzali B, Goldsmith DJA. Cardiac calcification in renal patients: what we do and don't know. Am J Kidney Dis. 2004;43:234–43. doi:10.1053/j.ajkd.2003.10.014.
2. Blancher J, Guerin AP, Pannier B, Marchais SJ, London GM. Arterial calcifications, arterial stiffness, and cardiovascular risk in end-stage renal disease. Hypertension. 2001;38:938–42. doi:10.1161/hy1001.096358.
3. Yeun JY, Levine RA, Mantadilok V, Kaysen GA. C-reactive protein predicts all-cause and cardiovascular mortality in hemodialysis patients. Am J Kidney Dis. 2000;35:469–76. doi:10.1016/S0272-6386(00)70200-9.
4. Block GA, Hulbert-Shearon TE, Levin NW, Port FK. Association of serum phosphorus and calcium x phosphate product with mortality risk in chronic hemodialysis patients: a national study. Am J Kidney Dis. 1998;31:607–17. doi:10.1053/ajkd.1998.v31.pm9531176.
5. Dorozhkin SV, Dorozhkina EI, Epple M. Precipitation of carbonateapatite from a revised simulated body fluid in the presence of glucose. J Appl Biomat Biomech. 2003;1:200–7.
6. Peters F, Epple M. Simulating arterial wall calcification in vitro: biomimetic crystallization of calcium phosphates under controlled conditions. Z Kardiol. 2001;90:81–5. doi:10.1007/s003920170047.
7. Boulet M, Marier JR. Precipitation of calcium phosphates from solutions at near physiological concentrations. Arch Biochem Biophys. 1961;93:157–65. doi:10.1016/0003-9861(61)90329-0.
8. Boskey AL, Posner AS. Formation of hydroxyapatite at low supersaturation. J Phys Chem. 1976;80:40–5. doi:10.1021/j100542a009.
9. Olsson L-F, Sandin K, Odselius R, Kloo L. In vitro formation of nanocrystalline carbonate apatite—a structural and morphological analogue of atherosclerotic plaques. Eur J Inorg Chem.2007;26:4123–7.doi:10.1002/ejic.200700654.
10. Sandin K, Kloo L, Odselius R, Olsson L-F. The observation of nano-crystalline calcium phosphate precipitate in a simple supersaturated inorganic blood serum model - composition and morphology. J Appl Biomat Biomech. 2009, in press.
11. C. Lentner (Ed). Geigy scientific tables 3. Ciba-Geigy: Basle; 1984.
12. Clase CM, Norman GL, Beecroft ML, Churchill DN. Albumin-corrected calcium and ionized calcium in stable haemodialysis patients. Nephrol Dial Transplant. 2000;15:1841–6. doi:10.1093/ndt/15.11.1841.
13. Fowler BO. Infrared studies of apatites. I. Vibrational assignments for calcium, strontium, and barium hydroxyapatites utilizing isotopic substitution. Inorg Chem. 1974;13:194–207. doi:10.1021/ic50131a039.
14. Nelson DGA, Williamson BE. Low-temperature laser Raman spectroscopy of synthetic carbonated apatites and dental enamel. Aust J Chem. 1982;35:715–27.
15. Fowler BO, Markovic M, Brown WE. Octacalcium phosphate. 3. Infrared and Raman vibrational spectra. Chem Mater. 1993;5:1417–23. doi:10.1021/cm00034a009.
16. Nelson DGA, Featherstone JDB. Preparation, analysis and characterization of carbonated-apatites. Calcif Tissue Int. 1982;34:69–81.
17. Pritzko W, Rentsch H. Structure refinement with X-ray powder diffraction data for synthetic calcium hydroxyapatite by Rietveld method. Cryst Res Technol. 1985;20:957–60. doi:10.1002/crat.2170200719.
18. Rössler S, Sewing A, Stölzer M, Born R, Scharnweber D, Dard M, et al. Electrochemically assisted deposition of thin calcium phosphate coatings at near-physiological pH and temperature. J Biomed Mater Res. 2003;64A:655–63. doi:10.1002/jbm.a.10330.
19. JCPDS (The Joint Committee on Powder Diffraction Standards) 2601 Park Lane, Swarthmore, PA; 1974.
20. Nancollas GH. The involvement of calcium phosphates in biological mineralization and demineralization processes. Pure Appl Chem. 1992;64:1673–8. doi:10.1351/pac199264111673.

21. Ostwald W. Studien über die Bildung und Umwandlung fester Körper. Z Phys Chem. 1897;22:289–330.
22. Wang HP, Feng XJ, Gou BD, Zhang TL, Xu SJ, Wang K. Effects of LDL, cholesterol, and their oxidized forms on the precipitation kinetics of calcium phosphates. Clin Chem. 2003;49:2027–36. doi:10.1373/clinchem.2003.024513.
23. Alberius Henning P, Moustiakimov M, Lidin S. Incommensurately modulated cadmium apatites. J Solid State Chem. 2000;150:154–8. doi:10.1006/jssc.1999.8571.
24. Becker A, Epple M, Muller KM, Schmitz I. A comparative study of clinically well-characterized human atherosclerotic plaques with histological, chemical, and ultrastructural methods. J Inorg Biochem. 2004;98:2032–8. doi:10.1016/j.jinorgbio.2004.09.006.
25. Tomazic BB. Physiochemical principles of cardiovascular calcification. Z Kardiol. 2001;90(Suppl 3):68–80. doi:10.1007/s003920170046.
26. Bigi A, Compostella L, Fichera AM, Foresti E, Gazzano M, Ripamonti A, et al. Structural and chemical characterization of inorganic deposits in calcified human mitral valve. J Inorg Biochem. 1988;34:75–82. doi:10.1016/0162-0134(88)85019-0.
27. Pawlikowski M, Pfitzner R, Wachowiak J. Mineralization (calcification) of coronary arteries. Mater Med Pol. 1994;26:3–8.
28. Kim H-M, Himeno T, Kokubo T, Nakamura T. Process and kinetics of bonelike apatite formation on sintered hydroxyapatite in a simulated body fluid. Biomaterials. 2005;26:4366–73. doi:10.1016/j.biomaterials.2004.11.022.
29. Robinson RA. An electron-microscopic study of the crystallite inorganic component of bone and its relationship to the organic matrix. J Bone Jt Surg. 1952;34A:389–436.
30. Holt C, van Kemenade MJJM, Harries JE, Nelson LS, Bailey RT, Hukins DWL, et al. Preparation of amorphous calcium-magnesium phosphates at pH 7 and characterization by x-ray absorption and Fourier transform infrared spectroscopy. J Cryst Growth. 1988;92:239–52. doi:10.1016/0022-0248(88)90455-1.
31. Shanahan CM, Cary NRB, Salisbury JR, Proudfoot D, Weissberg PL, Edmonds ME. Medial localization of mineralization-regulating proteins in association with Mönckeberg's sclerosis. Circulation. 1999;100:2168.
32. Moe SM, O'Neill KD, Duan D, Ahmed S, Chen NX, Leapman SB, et al. Medial artery calcification in ESRD patients is associated with deposition of bone matrix proteins. Kidney Int. 2001;61:638–47. doi:10.1046/j.1523-1755.2002.00170.x.
33. Stability Constants Database; IUPAC, Academic software, 2001.